CORROSION SCIENCE AND TECHNOLOGY, Vol.25, No.2(2026), pp.82~87
[Research Paper]
pISSN 1598-6462 / eISSN 2288-6524
DOI: https://doi.org/10.14773/cst.2026.25.2.82

Mechanical and Corrosive Properties of TiCrN Films Deposited by Direct-current, Mid-Frequency, and ICP Magnetron Sputtering

Sung-Yong Chun†

School of Mechanical and Ocean Engineering, Mokpo National University, Jeonnam 58554, Korea

(Received October 01, 2025; Revised October 17, 2025; Accepted October 20, 2025)

This study demonstrates the comparative properties of titanium chromium nitride (TiCrN) films deposited by direct current magnetron sputtering (dcMS), mid-frequency magnetron sputtering (mfMS), and inductively coupled plasma magnetron sputtering (ICPMS). The crystal structure and microstructure of the deposited films exhibited significant dependence on the sputtering mode employed. The introduction of mfMS and ICPMS deposition processes resulted in a transformation of the film morphology from a porous columnar structure to a denser configuration characterized by finer grains. The surface roughness and crystal grain size of the coated films were assessed using non-contact atomic force microscopy (AFM) and X-ray diffraction (XRD) analyses. A high-precision nanoindentation tester was utilized to measure the nanohardness and elastic modulus of the TiCrN films deposited by three sputtering techniques: dcMS, mfMS, and ICPMS. Additionally, to conduct a comparative analysis of the effects of the sputtering modes on the corrosion resistance of the TiCrN films, a potentiodynamic polarization test was performed, allowing for evaluation of these effects through electrochemical analysis.

Keywords: *Direct current magnetron sputtering, Mid-frequency magnetron sputtering, Inductively coupled plasma assisted magnetron sputtering, TiCrN, Films*

1. Introduction

Binary metal nitride hard coatings, such as TiN and CrN films, are currently used as protective coatings in various industries owing to their high hardness, low coefficient of friction, and ability to extend tool life even in harsh environments [1,2]. However, the performance and reliability of these nitride coatings fails to meet the requirements in certain applications such as high-speed machining, dry cutting, drilling, and jet engine turbine blades [3]. Consequently, ternary metal nitride coatings, such as TiCrN films, have gained considerable attention owing to the combined properties of TiN and CrN. In general, CrN is reported to have higher corrosion resistance than TiN [4], but TiCrN has been reported to exhibit better corrosion resistance to seawater than CrN [5]. In terms of mechanical properties, TiCrN films have also been found to exhibit higher hardness than TiN thin films (21 GPa) and CrN (19 GPa) coatings [5]. Furthermore, the synthesis of ternary compound coatings has been reported to generate (i) multiphase structures (often leading to fine grains and distorted morphologies [6]) and (ii) ternary nitrides with superior mechanical properties compared with binary nitrides [7].

The microstructure and hardness of ternary hard coatings are sensitively affected by the energy and density of the ion flux in the depositing plasma [8]. The ion flux mainly comprises Ar^+ or N^{2+}, and for typical direct current magnetron sputtering (dcMS), the ionization rate of sputtered species is typically less than 1% [9]. This affects not only the composition of the coatings but also their crystal structure and mechanical properties. To date, no studies have reported the effects of plasma-assisted sputtering modes, such as mid-frequency magnetron sputtering (mfMS) and inductively coupled plasma magnetron sputtering (ICPMS), on the properties of TiCrN films in comparison with conventional dcMS. Therefore, this study will present results comparing mechanical hardness and corrosion resistance reported in other literature. In this study, three types of TiCrN films were deposited using dcMS, mfMS, and ICPMS in the same vacuum chamber while keeping all process parameters

†Corresponding author: sychun@mnu.ac.kr
Sung-Yong Chun: Professor

constant. The effects of the different sputtering modes on the crystal structure, microstructure, mechanical properties, and corrosion resistance of TiCrN films were systematically investigated.

2. Experimental Method

Three types of TiCrN thin films were deposited using dcMS with direct current, mfMS with pulsed direct current, and ICPMS with inductively coupled plasma, as listed in Table 1. The starting materials were a 99.95% pure TiCr target with a diameter of 3" and a thickness of 1/4" and ultrahigh purity Ar and N_2 gases. Through preliminary experiments, the Ar and N_2 gas flow rates were set to 20 sccm each to produce single-phase TiCrN thin films. During deposition, the distance between the substrate and the target was maintained at 60 mm and the substrate was rotated at a speed of approximately 10 rpm to achieve uniform coating. An N-type Si(100) single-crystal wafer with a diameter of 4" was used as a substrate material, and its surface impurities were removed via ultrasonic cleaning in acetone and ethanol for 10 min each. In addition, Ar plasma cleaning was performed to remove organic contaminants. The initial pressure in the vacuum chamber was set to approximately 1.4×10^{-4} Torr using a rotary pump and a turbomolecular pump, while the total process pressure ($Ar+N_2$) was maintained at 2 mTorr. High-resolution X-ray diffraction (XRD) (PAN analytical/X'pert-pro MRD) was used to analyze the crystal structure of the obtained TiCrN thin films, and field emission scanning electron microscopy (FE-SEM) (Hitachi/S-3500N) was used to examine their surface and cross-sectional microstructure. Auto probe atomic force microscopy (AFM) (Park Systems/Park NX15) was used to measure the surface roughness of the thin films. Nanoindentation Tester (NHT3, Anton Paar) was used for the higher force instrumented indentation testing of thin film.

Table 1. Sputtering type for deposition of TiCrN films prepared by dcMS, mfMS and ICPMS

Conditions	1	2	3
Sputtering (type)	dcMS	mfMS	ICPMS
Sputtering Power (W)	500	500	500
ICP Power (W)	-	-	100
Pulse frequency (kHz)	-	15	-
Duty cycle (%)	-	75	-
Substrate temperature (℃)	100	100	100
Thickness (nm)	368	392	389

Visual matrices of indentations and continuous multi cycles (CMC) were conducted to measure the mechanical properties as a function of position on the surface and depth in the sample. For electrochemical evaluation of the corrosion properties of the TiCrN films, potentiodynamic polarization tests were performed using an electrochemical workstation (VSP, BioLogic). To ensure the reproducibility of the experiments, the tests were repeated at least three times under the same conditions using a 3.5% aqueous NaCl solution with a scan range of -0.8 to 1.0 V and a scan rate of 0.01 V/s.

3. Results and Discussion

3.1 Crystal structure

The results of X-ray diffraction analysis of the TiCrN films deposited using three sputtering modes such as dcMS, mfMS and ICPMS are shown in Fig. 1. For comparison, the (111), (200), and (220) peaks of the standard TiN sample (JCPDS No. 87-0633) and the standard CrN sample (JCPDS No. 77-0047) are shown in Fig. 1 with dotted and solid lines. These peaks are observed for all the TiCrN thin films obtained. The

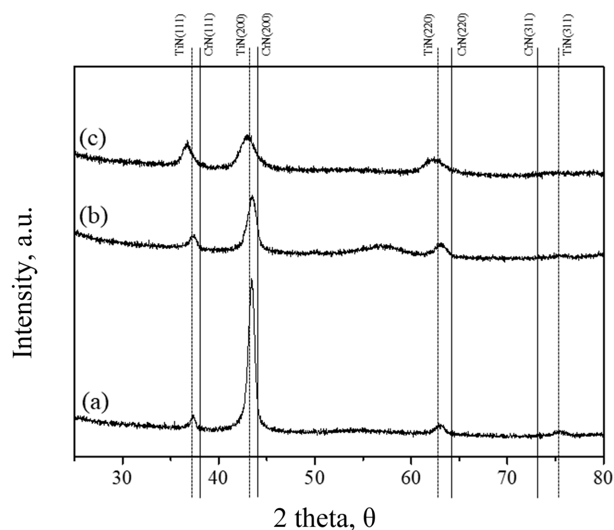

Fig. 1. XRD patterns of the as-prepared TiCrN films prepared by (a) dcMS, (b) mfMS and (c) ICPMS

diffraction peaks of the films are located at approximately 36.78° ~ 37.25°, 42.96 ° ~ 43.60°, and 61.73° ~ 62.90°. In other words, the positions of these peaks align with those of the JCPDS peaks of the standard TiN and CrN samples (i.e., the (100), (200), and (220) peaks).

Furthermore, the full width at half maximum (FWHM) of the (111) peak of the TiCrN film successively deposited via mfMS and ICPMS shows an increase compared with that of the TiCrN film deposited via dcMS. The average crystal grain size was calculated from the (111) peak using the Scherrer equation [10], showing that the average crystal grain sizes of the TiCrN thin films deposited via dcMS, mfMS, and ICPMS were 12.0, 8.2, and 5.0 nm, respectively, with a decrease of up to 58% for ICPMS compared to dcMS.

3.2 Microstructure

The microstructures of TiCrN films deposited by three sputtering modes such as dcMS, mfMS, and ICPMS were observed using FE-SEM. Fig. 2 shows the surface and cross-sectional images of each film. The surface images of the TiCrN films show that those deposited by mfMS and ICPMS consist of small, rounded grains with a uniform size distribution and dense packing, in contrast to the films deposited via dcMS.

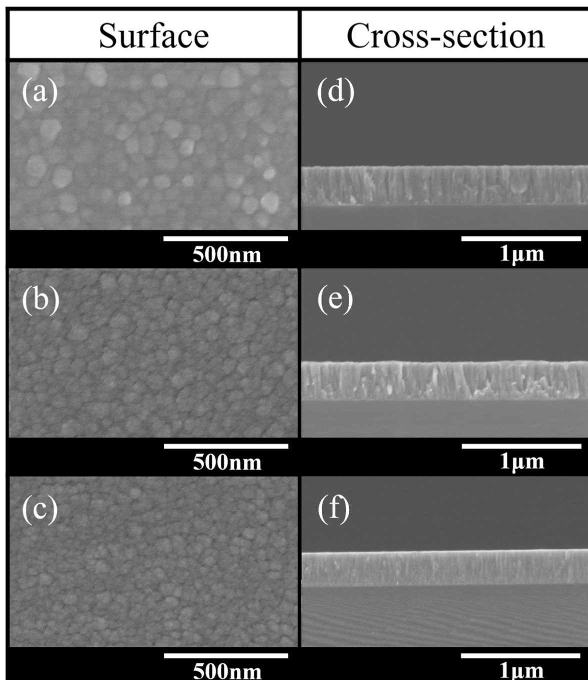

Fig. 2. Microstructure through FE-SEM for the TiCrN film surface [(a) dcMS, (b) mfMS and (c) ICPMS] and cross-sectional FE-SEM [(d) dcMS, (e) mfMS and (f) ICPMS]

In contrast, the TiCrN film deposited by dcMS exhibits countless randomly distributed, pebble-like rounded grains of varying sizes, accompanied by numerous intergranular voids. Moreover, cross-sectional image comparison of the TiCrN films reveals that those deposited via ICPMS exhibit a dense, void-free microstructure with negligible interparticle spacing. In contrast, the TiCrN film deposited by dcMS exhibited columnar crystallites with clearly defined grain boundaries.

Non-contact AFM analysis was conducted to examine the effects of dcMS, mfMS, and ICPMS deposition modes on the surface roughness of TiCrN films. Fig. 3 shows the surface roughness (Ra) and there is a close correlation between the sputtering deposition process and the surface roughness of the films. The surface roughness of the TiCrN films deposited by dcMS, mfMS, and ICPMS was 3.6, 3.1, and 2.0 nm, respectively, representing a 44.4% reduction for ICPMS compared to dcMS. It is suggested that the generation of high-energy ions when using mfMS and ICPMS increased the kinetic energy of the charged particles traveling from the target surface to the substrate and enhanced their adatom mobility even after reaching the substrate surface, leading to flattening of the thin film surface.

3.3 Nanoindentation Hardness and Elastic Modulus

A high-precision nanoindentation tester was used to

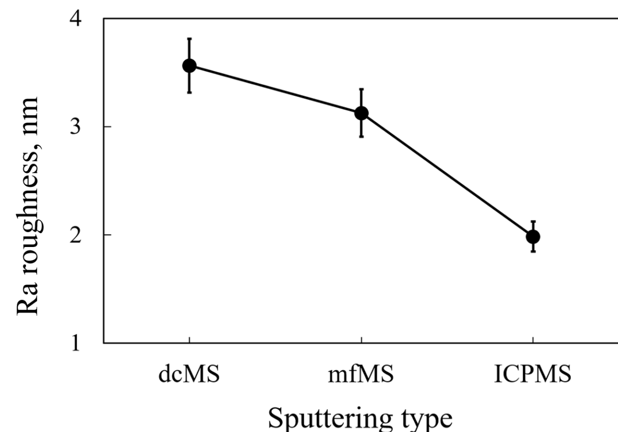

Fig. 3. Ra roughness of TiCrN films prepared by dcMS, mfMS and ICPMS

measure the nanohardness and elastic modulus of the TiCrN films deposited by three sputtering modes such as dcMS, mfMS and ICPMS. The average values obtained from measurements at over 30 locations with 1 μm spacing per sample are shown in Fig. 5. Owing to the nanoindentation size effect, it is challenging to obtain precise hardness measurements of thin films a few hundred nanometers thick using a conventional micro-Vickers hardness tester. Therefore, in this study, quantitative nanohardness measurements were conducted according to the standard method of instrumented nanoindentation specified in ISO 14577. In particular, the applied load for nanohardness measurements of the thin films was set to 5 mN, and the hardness values were averaged at an indentation depth corresponding to 1/10 of the total film thickness to eliminate the indentation size effect, which tends to increase the measured hardness as the indentation depth decreases [11].

Fig. 4 shows the results of nanoindentation hardness and elastic modulus of the TiCrN films deposited by dcMS, mfMS, and ICPMS. The nanoindentation hardness of the TiCrN films deposited by dcMS, mfMS, and ICPMS was 13.3, 18.0, and 26.1 GPa, respectively, while the elastic modulus was 117.5, 140.1, and 206.8 GPa, respectively. The nanoindentation hardness and the elastic modulus increase in the order of dcMS, mfMS, and ICPMS. In other words, the nanoindentation hardness and elastic modulus of the TiCrN thin film deposited via ICPMS increased by 96% and 76%, respectively, compared to that of the thin film deposited via dcMS.

The mechanical hardness of TiCrN films reported in recent literature is 10–20 GPa [8]. This is similar to the hardness of the TiCrN films obtained by dcMS and mfMS in this study, but is 38–77% lower than the results obtained by ICPMS. These results are highly consistent with the Hall-Petch effect [12]. According to the Hall-Petch relationship, a reduction in the crystal grain size of hard metals decreases the grain boundary voids, thereby enhancing their mechanical hardness. As discussed earlier, SEM and AFM analyses indicate that smaller crystal grains are formed depending on the sputtering mode. Therefore, both the Hall-Petch effect and the results obtained from the SEM and AFM analyses corroborate that the hardness of the TiCrN thin films increases as the film deposition mode changes from dcMS to mfMS and ICPMS.

3.4 Electrochemical Properties

To comparatively analyze the effects of the sputtering modes on the corrosion resistance of TiCrN film, a potentiodynamic polarization test that enables the effects to be evaluated with an electrochemical experiment was conducted [13]. For more accurate measurement, the conductive silver made line was grounded to the measuring electrode for the potential polarization test. In a specific method, a conductive silver paste was used to connect to the end of the surface of the TiCrN film, and all parts except for the exposed test surface of the film having an area of 1 cm^2 were covered with silicon.

Fig. 5 shows the polarization curve for Tafel analysis after the potentiodynamic polarization test. When the

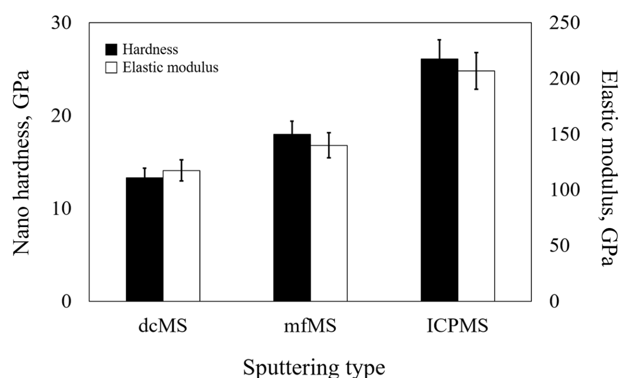

Fig. 4. Nanoindentation hardness and elastic modulus of TiCrN films prepared by dcMS, mfMS and ICPMS

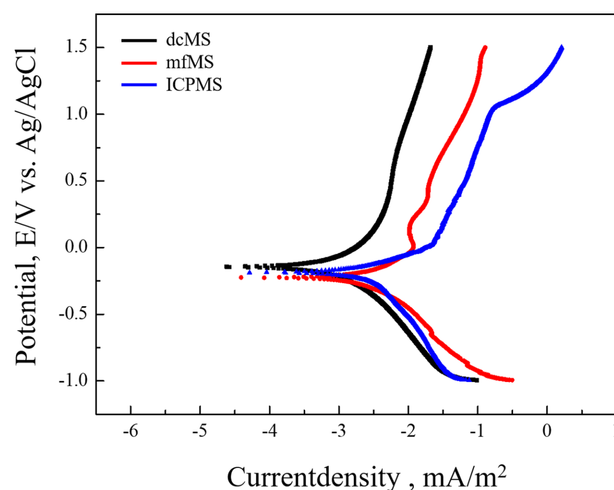

Fig. 5. Potential, E/V vs Ag/AgCl of TiCrN films prepared by dcMS, mfMS and ICPMS

effects of the sputtering modes on the corrosion potential of TiCrN film are compared, the corrosion potential of TiCrN film prepared by dcMS, mfMS and ICPMS was -0.145 V, -0.226 V and -0.187 V, respectively. It means that the corrosion potentials of TiCrN films deposited by mfMS and ICPMS were more active than those of TiCrN film deposited by dcMS. However, when the effects of the sputtering modes on the corrosion current density of TiCrN film are compared, the corrosion current densities of TiCrN films deposited by mfMS and ICPMS were about 5.3×10^{-6} mA/cm^2 and 4.2×10^{-6} mA/m^2, respectively. These values are 1.6 ~ 2.0 times higher than 2.6×10^{-6} mA/cm^2, the corrosion current density of TiCrN film prepared by dcMS. It means that the corrosion current density of the films deposited by mfMS and ICPMS has not been greatly improved compared to the film deposited by dcMS. The reasons for these results will be studied through further experiments such as electrochemical impedance spectroscopy (EIS) varying film thickness and substrate temperature in the future.

4. Conclusion

In this study, three types of cubic fcc nanocrystalline TiCrN films were deposited using dcMS, mfMS, and ICPMS, which employ direct current, mid-frequency, and inductively coupled plasmas, respectively. On the surface of the TiCrN thin films deposited by dcMS, round, pebble-like particles of varying sizes were randomly distributed, whereas the cross section exhibited porous, columnar crystal grains. Meanwhile, the thin films deposited by mfMS and ICPMS exhibited surfaces composed of fine, spherical particles and denser cross-sectional microstructures. The average crystal grain size of the TiCrN thin films deposited by dcMS, mfMS, and ICPMS decreased to 3.6, 3.1, and 2.0 nm, respectively, while the nanoindentation hardness and elastic modulus increased from 13.3 to 26.1 GPa and from 117.5 to 206.8 GPa, respectively, in the order of dcMS, mfMS, and ICPMS. This study demonstrates that the properties of TiCrN films can be strongly affected by the conditions of the sputter deposition process. Effect of the sputtering mode on the corrosion behavior of TiCrN films was also investigated by potentiostatic polarization experiments. The corrosion potentials of the TiCrN films deposited by mfMS and ICPMS were -0.226 V and -0.187 V, respectively, which were lower than -0.145 V of the films deposited by dcMS, but the corrosion current densities of the films deposited by mfMS and ICPMS were slightly higher (5.3×10^{-6} mA/m^2 and 4.2×10^{-6} mA/m^2) than those of the films deposited by dcMS (2.6×10^{-6} mA/m^2).

Acknowledgments

This work was supported by the Regional Innovation System and Education (RISE) initiative, funded by the Ministry of Education and Jeollanam-do, Republic of Korea.

References

1. S. Y. Chun, J. Y. Hwang, Effects of Duty Cycle and Pulse Frequency on the Microstructure and Mechanical Properties of TiAlN Coatings, *Journal of the Korean Ceramic Society*, **51,** 447 (2014). Doi: https://doi.org/10.4191/kcers.2014.51.5.447
2. S. Y. Chun, S. J. Kim, Enhancement of the Corrosion Resistance of CrN Film Deposited by Inductively Coupled Plasma Magnetron Sputtering, *Corrosion Science and Technology*, **20**, 112 (2021). Doi: https://doi.org/10.14773/cst.2021.20.3.112
3. S. Y. Chun, Microstructure and Mechanical Properties of Nanocrystalline TiN Films Through Increasing Substrate Bias, *Journal of the Korean Ceramic Society*, **47,** 479 (2010). Doi: https://doi.org/10.4191/kcers.2010.47.6.479
4. L. Wang, D. O. Northwood, X. Nie, J. Housden, E. Spain, A. Leyland, A. Matthews, Corrosion properties and contact resistance of TiN, TiAlN and CrN coatings in simulated proton exchange membrane fuel cell environments, *Journal of Power Sources*, **195**, 3814 (2010). Doi: https://doi.org/10.1016/j.jpowsour.2009.12.127
5. M. A. Ezazi, M. M. Quazi, E. Zalnezhad, Ahmed A. D. Sarhan, Enhancing the tribo-mechanical properties of aerospace AL7075-T6 by magnetron-sputtered Ti/TiN, Cr/CrN & TiCr/TiCrN thin film ceramic coatings, *Ceramics International*, **40**, 15603 (2014). Doi: https://doi.org/10.1016/j.ceramint.2014.07.067
6. F. Ge, P. Zhu, F. Meng, Q. Xue and F. Huang, Achieving Very Low Wear Rates in Binary Transition-Metal Nitrides: The Case of Magnetron Sputtered Dense and Highly Oriented VN Coatings, *Surface and Coatings Technology*, **248**, 81 (2014). Doi: https://doi.org/10.1016/j.surfcoat.2014.03.035

7. K. V. Chauhana, S. K. Rawal, A review paper on tribological and mechanical properties of ternary nitride based coatings, *Procedia Technology*, **14,** 430 (2014). Doi: https://doi.org/10.1016/j.protcy.2014.08.055
8. A. Kehal, N. Saoula, S-E-H. Abaidia, C. Nouveau, Effect of Ar/N2 flow ratio on the microstructure and mechanical properties of Ti-Cr-N coatings deposited by DC magnetron sputtering on AISI D2 tool steels, *Surface and Coatings Technology*, **421**, 127444 (2021). DOI: https://doi.org/10.1016/j.surfcoat.2021.127444
9. S. G. Rao, R. Shu, R. Boyd, A. Febvrier, P. Eklund, Plasma diagnostics and film growth of multicomponent nitride thin films with magnetic-field-assisted-dc magnetron sputtering, *Vacuum*, **204**, 111331 (2022). Doi: https://doi.org/10.1016/j.vacuum.2022.111331
10. S. Nasiri, M. Rabiei, A. Palevicius, G. Janusas, A. Vilkauskas, V. Nutalapati, A. Monshi, Modified Scherrer equation to calculate crystal size by XRD with high accuracy, examples Fe_2O_3, TiO_2 and V_2O_5, *Nano Trends*, **3**, 100015 (2023). Doi: https://doi.org/10.1016/j.nwnano.2023.100015
11. P. Wang, Y. Gao and P. Wang, A comparative study of indentation size effect models for different materials, *Scientific Reports*, **14**, 20010 (2024). Doi: https://doi.org/10.1038/s41598-024-71136-5
12. Y. Li, A. J. Bushby and D. J. Dunstan, The Hall–Petch effect as a manifestation of the general size effect, *Proceedings of the Royal Society A*, **472**, 2190 (2016). Doi: https://doi.org/10.1098/rspa.2015.0890
13. Sung-Yong Chun and Seong-Jong Kim, Enhancement of the Corrosion Resistance of CrN Film Deposited by Inductively Coupled Plasma Magnetron Sputtering, *Corrosion Science and Technology*, **20**, 112 (2021). Doi: https://doi.org/10.14773/cst.2021.20.3.112